Electronic properties of Ba$_{1-x}$Sr$_x$V$_{13}$O$_{18}$ ($x = 0, 0.2, 1$) studied using hard x-ray photoelectron spectroscopy

S. Dash,[1] M. Okawa,[2] T. Kajita,[3] T. Yoshino,[1] R. Shimoyama,[2] K. Takahashi,[2] Y. Takahashi,[2] R. Takayanagi,[2] T. Saitoh,[2]
D. Ootsuki,[4] T. Yoshida,[4] E. Ikenaga,[5] N. L. Saini,[6] T. Katsufuji,[3] and T. Mizokawa[1]

[1]*Department of Applied Physics, Waseda University, Shinjuku, Tokyo 169-8555, Japan*
[2]*Department of Applied Physics, Tokyo University of Science, Katsushika, Tokyo 125-8585, Japan*
[3]*Department of Physics, Waseda University, Shinjuku, Tokyo 169-8555, Japan*
[4]*Department of Interdisciplinary Environment, Kyoto University, Sakyo, Kyoto 606-8501, Japan*
[5]*Japan Synchrotron Radiation Research Institute, Sayo, Hyogo 679-5198, Japan*
[6]*Department of Physics, University of Roma "La Sapienza" Piazzale Aldo Moro 2, 00185 Roma, Italy*

We have studied the electronic structure of Ba$_{1-x}$Sr$_x$V$_{13}$O$_{18}$ ($x = 0, 0.2, 1$) at different temperatures across the trimerization and charge-order transitions using hard x-ray photoemission spectroscopy (HAXPES). The V $2p$ HAXPES indicates V^{2+}/V^{3+} charge order and fluctuation in the high-temperature tetramer phase, low-temperature trimer phase, and intermediate-temperature charge-order phase in the series of $x = 0, 0.2, 1$. In the valence-band HAXPES, although the spectral weight at the Fermi level tends to be suppressed in all the phases due to strong charge order or fluctuation, it increases in the trimer phase at $x = 0.2$, in agreement with the decrease of resistivity and the increase of itinerant electrons in the trimer phase. Interestingly, in the most conducting $x = 1$ without the charge-order phase, the spectral weight at the Fermi level is strongly suppressed even in the trimer phase, indicating that charge fluctuation in the trimer phase is different between $x = 0.2$ and 1.

I. INTRODUCTION

The 3d transition-metal oxides exhibit various interesting physical properties such as metal-insulator transition (MIT), colossal magnetoresistance, and spin-charge-orbital ordering [1]. The origin of such behaviors is quite attractive and compelling to understand. Among them, there are various origins of insulating states in transition-metal oxides, including on-site Coulomb interaction for Mott insulators with integer-number valence, intersite Coulomb interaction for charge-order insulators with non-integer-number valence, Peierls transition with structural distortion, and Anderson localization with disorder effect. The MITs are usually accompanied by spin and/or charge and/or orbital ordering of 3d electrons. For the case of orbital ordering with integer number of valence, there are several differences between the orbital orderings in LaMnO$_3$ and LiVO$_2$: in LaMnO$_3$, the electrons responsible for the orbital ordering exist at each Mn site, whereas in LiVO$_2$, the electrons exist at each V-V bond. Furthermore, in LaMnO$_3$, the electron with orbital degrees of freedom also has spin degrees of freedom, whereas in LiVO$_2$, the spin degrees of freedom are suppressed by the spin-singlet bond formation [2]. Such spin-singlet trimers are common building blocks for the V^{3+} oxidation state on the triangle-based lattice [3,4].

Ba$_{1-x}$Sr$_x$V$_{13}$O$_{18}$ and BaV$_{10}$O$_{15}$ are among this category [5,6] with orbital degree of freedom like LaMnO$_3$ and with trimerization like LiVO$_2$. In addition, among the various charge-ordering phenomena, the charge order with V^{2+} and V^{3+} sites in Ba$_{1-x}$Sr$_x$V$_{13}$O$_{18}$ [5,6] and BaV$_{10}$O$_{15}$ [7,8] is quite rare compared to the V^{3+} and V^{4+} charge-order insulating state in various vanadates [9–13]. BaV$_{10}$O$_{15}$ forms a triangle-based lattice with a structural phase transition with anomaly of electrical conductivity at around 130 K. Electronic properties of BaV$_{10}$O$_{15}$ were recently reported with V^{2+} and V^{3+} charge ordering [7] with V trimerization. Other studies have also been obtained from the resonant x-ray scattering

experiments [14], V nuclear magnetic resonance (NMR) [15] as proposed by Pen *et al.* [16], time-resolved spectroscopy [17], and Raman spectroscopy [18]. On the other hand, there are a few studies on Ba$_{1-x}$Sr$_x$V$_{13}$O$_{18}$. Ba$_{1-x}$Sr$_x$V$_{13}$O$_{18}$ forms a rock-salt lattice with periodically missing V and O sites [19,20], and V atoms are on the fcc lattice as the stacking of the triangular lattices with the ABCABC periodicity along the diagonal direction. The side view of the crystal structure of BaV$_{13}$O$_{18}$ parallel to the ab plane is shown in Fig. 1(a) and the top view along the c axis is shown in Fig. 1(b). Ikeda and co-workers have found that the low-temperature phase is dominated by V trimers [Fig. 1(c)] and high-temperature phase by V tetramers [Fig. 1(d)] in the series of Ba$_{1-x}$Sr$_x$V$_{13}$O$_{18}$ for $0 \leqslant x \leqslant 1$ [5,6].

The schematic of the temperature-dependent phase transition from V tetramers to V trimers is shown in Fig. 2(a). There is a strong competition between the tetramer phase and the trimer phase in the series of Ba$_{1-x}$Sr$_x$V$_{13}$O$_{18}$, and the electronic structure substantially changes in association with the phase transition. T_{tr} corresponds to the transition temperature from the tetramer to trimer phase. BaV$_{13}$O$_{18}$ takes the same crystal structure as that of SrV$_{13}$O$_{18}$ and exhibits an intermediate charge-order phase followed by the low-temperature trimer phase. The charge-order phase exists for lower values of x (0–0.3) in Ba$_{1-x}$Sr$_x$V$_{13}$O$_{18}$. T_{co} is defined as the transition temperature to the intermediate charge-order phase. Although the details of the crystal structure and the transport properties (including resistivity ρ, magnetic susceptibility χ, Seebeck coefficient S, and thermal conductivity K) of Ba$_{1-x}$Sr$_x$V$_{13}$O$_{18}$ have been reported [5,6], here we study the electronic structure and the valence state of Ba$_{1-x}$Sr$_x$V$_{13}$O$_{18}$ using spectroscopic methods. The schematics of resistivity ρ [Fig. 2(b)], Seebeck coefficient S [(Fig. 2(c)], and magnetic susceptibility χ [(Fig. 2(d)] across the transition temperatures are drawn for $x = 0, 0.2, 1$. These
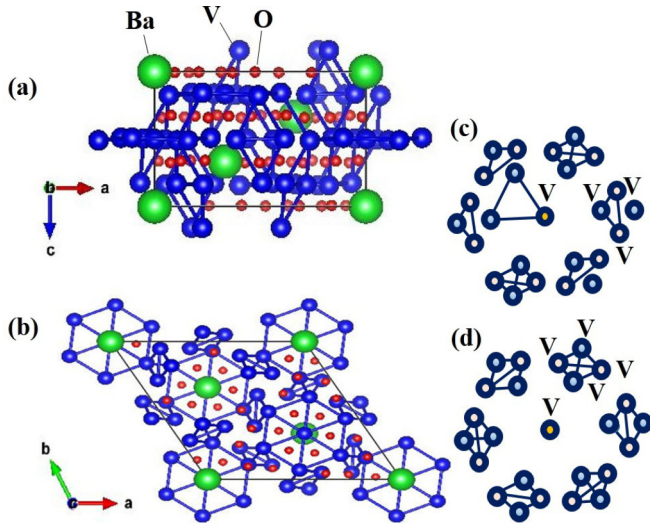
FIG. 1. The crystal structure of $BaV_{13}O_{18}$ (a) along the hexagonal *ab* plane and (b) from the *c* axis is drawn from Iwasaki *et al.* [19], using VESTA [21]. (c) The schematics of the low-temperature trimer phase and (d) high-temperature tetramer phase of V atoms. Barium, vanadium, and oxygen atoms are shown by filled circles with different colors.

properties are associated with the presence of tetramers in the high-temperature phase and trimers in the low-temperature phase. The intermediate-temperature charge-order phase is also dominated with tetramers and shows interesting physical behaviors [5,22]. Since the average valence of V is $\sim +2.62$, $Ba_{1-x}Sr_xV_{13}O_{18}$ is expected to show an interesting interplay between V charge order and fluctuation with V trimerization or tetramerization. It has been proposed that the high-temperature phase contains 31 electrons within 3 tetramers (10 electrons per tetramer) and centrally localized V^{4+} (one electron). The low-temperature phase contains three trimers and one tetramer, i.e., $31 - (3 \times 6 + 10) = 3$ itinerant $3d$ electrons that have a metallic nature [6].

In order to clarify the electronic structural change across the phase transitions and to reveal the relationship between the V tetramers or trimerization and the rare V^{2+} and V^{3+} charge ordering, we have performed hard x-ray photoemission spectroscopy (HAXPES) of $Ba_{1-x}Sr_xV_{13}O_{18}$. Since charge-ordered systems tend to exhibit surface electronic states different from bulk ones, HAXPES is more important to understand the bulk properties and hence useful to compare with the previously studied bulk characterizations such as magnetic and transport properties [5,6]. Although there is a disadvantage of low cross section with high photon energies, it is more reliable because the information is coming from the bulk irrespective of surface condition. On the other hand, angle-resolved photoemission spectroscopy with low photon energies is surface sensitive and useful to study layered materials with a well-defined cleavage plane. Since the present system has no well-defined cleavage plane, surface-sensitive experiments with soft x ray are not appropriate to compare with bulk sensitive measurements. The V $2p$ spectrum is split into two components at the high-temperature tetramer, the low-temperature trimer, and intermediate-temperature charge
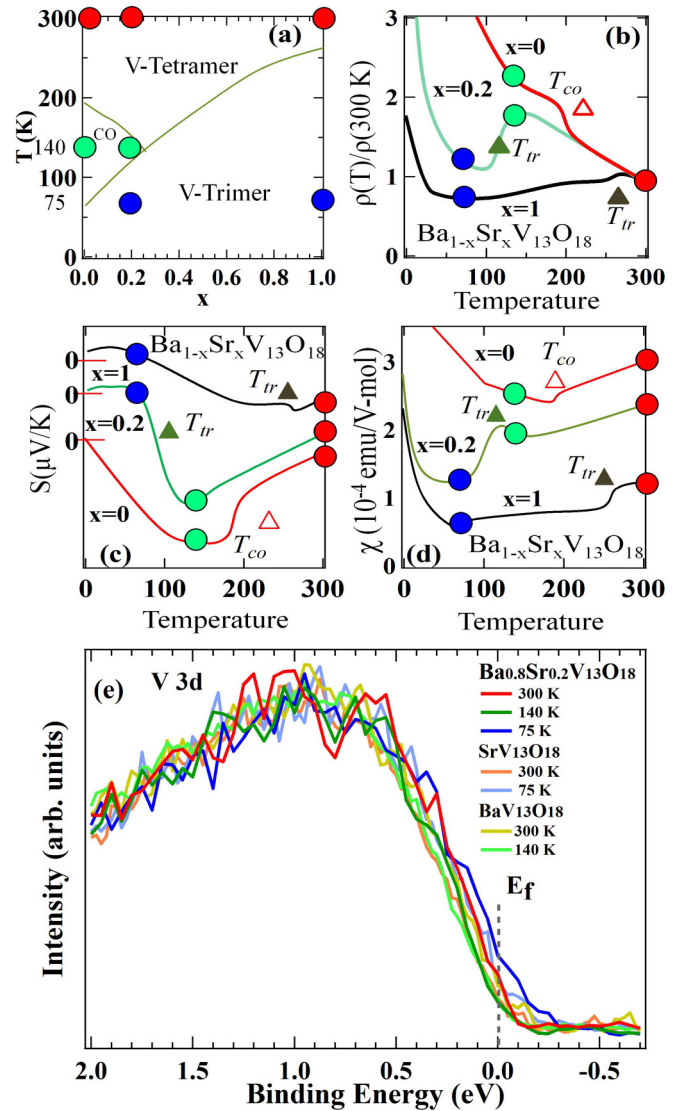

FIG. 2. The schematics of (a) phase diagram for V tetramer to V trimer and charge-order phases, (b) resistivity ρ, (c) Seebeck coefficient S, (d) magnetic susceptibility χ for $AV_{13}O_{18}(A = Ba,Sr)$, and mixed compound $Ba_{0.8}Sr_{0.2}V_{13}O_{18}$ obtained from Ikeda *et al.* [6]. T_{tr} is shown with a filled triangle and T_{co} is shown with an open triangle. Each circle indicates the temperature for the HAXPES measurement. (e) Valence-band HAXPES spectra collected around the V $3d$ region.

order phases for $x = 0, 0.2, 1$, indicating the presence of V^{2+} and V^{3+} charge fluctuation and charge order (V^{2+} and V^{3+} ratio is approximately $5:8$). Based on the proposed charge order or fluctuation, the relationship between the electronic properties and various physical properties will be discussed.

II. EXPERIMENTAL DETAILS

The single crystals of $Ba_{1-x}Sr_xV_{13}O_{18}$ ($x = 0, 0.2, 1$) were grown as reported in the literature [5,6]. HAXPES measurements were performed at BL09XU of SPring-8 [23]. HAXPES with 7930 eV of source energy gives more bulk information with probing depth around 10 nm [24–27]. The incidence

and detection angles are set to about 10 and 90 degrees, respectively, to increase photoelectron yield. The surface contamination was removed by fracturing the single crystals under ultrahigh vacuum of 10^{-6} Pa at 300 K. The electronic state of the topmost surface layer (width of about 1 nm) would be different from that of the bulk. With the probing depth around 10 nm, more signals (above 90 percent) are expected from the bulk region [28]. Sample charging effects are removed with conducting carbon surroundings. Photoelectrons excited with photon energy of 7930 eV were collected and analyzed by Omicron-Scienta R4000. With such high photon energy, the cross sections at the O 1s and V 2p edges are decreased by a magnitude of 148.148 and 221.694 times, respectively, from those with Al Kα source [29]. On the contrary, the advantages of HAXPES measurements are bulk sensitivity and high resolution with the third-generation synchrotron light sources (SPring-8). The pass energy was set to 200 eV and the total-energy resolution was about 270 meV. The binding energy was calibrated using the Fermi edge of Au reference.

III. RESULTS AND DISCUSSION

Figure 2(e) shows the HAXPES results collected across V 3d of $AV_{13}O_{18}$ (A = Ba,Sr), $Ba_{0.8}Sr_{0.2}V_{13}O_{18}$ at different temperatures across the transitions. Each spectrum is normalized with the V 3d intensity (total area). First, the spectral weight at the Fermi level tends to be suppressed in all the compositions and the temperatures. The spectral weight suppression would be related to the charge order or fluctuation obtained from the V 2p HAXPES that will be discussed later.
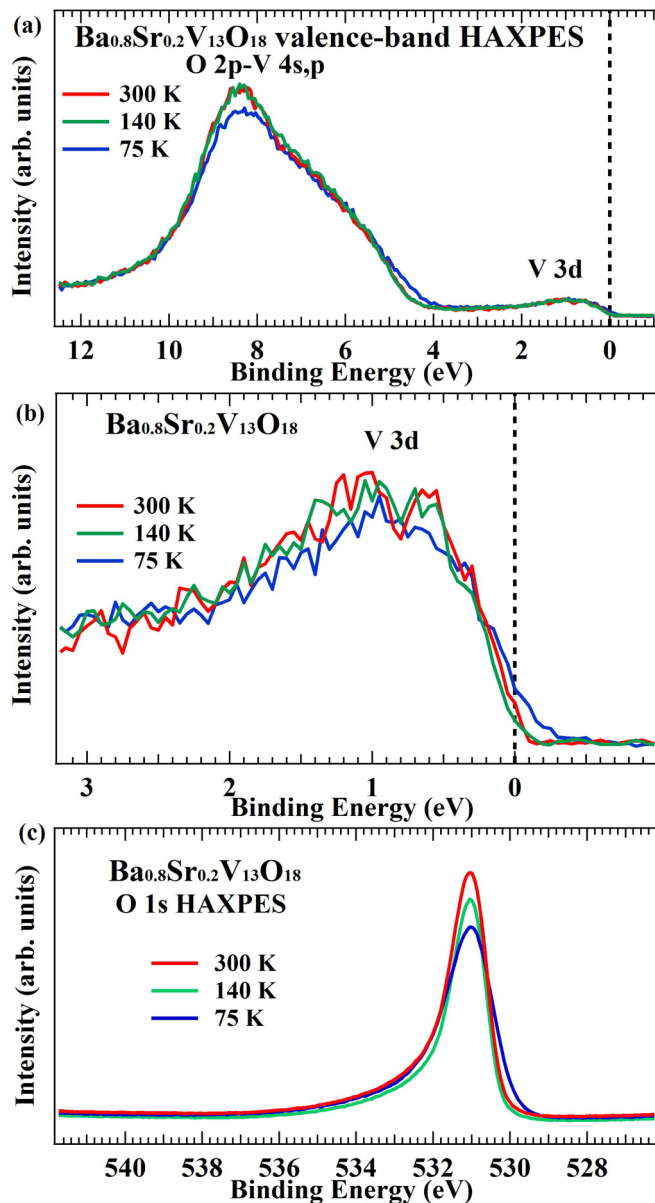

FIG. 3. HAXPES spectra of $Ba_{0.8}Sr_{0.2}V_{13}O_{18}$ at 300, 140, and 75 K for (a) valence band, (b) V 3d, and (c) O 1s.
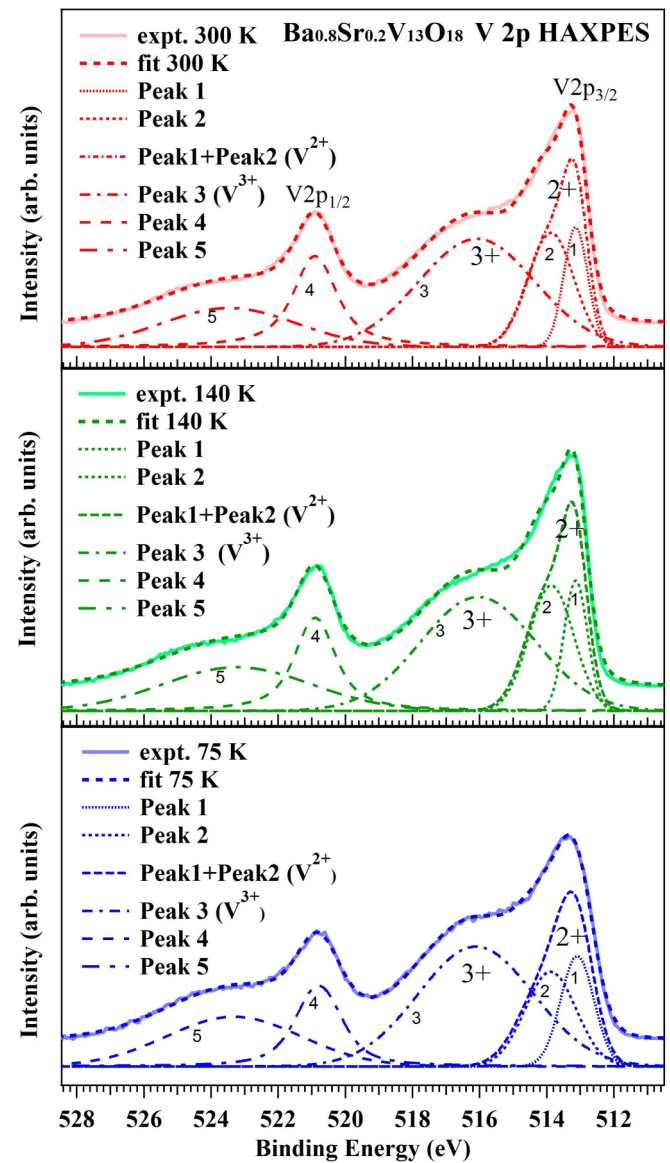

FIG. 4. V 2p HAXPES spectra fitted with five Voigt functions for 300, 140, and 75 K. Peaks 1 and 2 represent V^{2+}, and peak 3 represents the V^{3+} component in the V 2$p_{3/2}$. Peaks 4 and 5 are fitted for the V 2$p_{1/2}$ region. Peaks 1 and 2 of V 2$p_{3/2}$ collected at 75 K are broadened and shifted towards the lower binding energy side.

The spectral weight at the Fermi level is slightly enhanced for $Ba_{0.8}Sr_{0.2}V_{13}O_{18}$ and $SrV_{13}O_{18}$ at 75 K. This enhancement could be the signature of the metallic trimer phase due to itinerant $3d$ electrons. However, spectral weight across the Fermi edge of $SrV_{13}O_{18}$ collected at 75 K is relatively suppressed compared to $Ba_{0.8}Sr_{0.2}V_{13}O_{18}$. The valence-band HAXPES spectra of $Ba_{1-x}Sr_xV_{13}O_{18}$ for $x = 0.2$ are shown in Figs. 3(a) and 3(b). In the high-temperature phase (300 K) and the intermediate-temperature charge-order phase (140 K), the spectral weight at the Fermi level is strongly suppressed, likely with a pseudogap that can be associated with the tetramer formation and the charge order. On the other hand, the spectral weight at the Fermi level is enhanced at 75 K, indicating that the number of the itinerant electrons is increased in the trimer phase. However, the pseudogap still remains and can be related to the charge fluctuation in the trimer phase observed by the V $2p$ HAXPES. The increase in spectral weight at the Fermi level can be comparable with the decreases in resistivity [Fig. 2(b)] and the behavior of Seebeck coefficient S approaching zero [Fig. 2(c)]. The O $1s$ HAXPES is shown in Fig. 3(c). The O $1s$ can be fitted to a Doniach-Sunjic profile (see Supplemental Material [30]).

Figure 4 shows the V $2p$ HAXPES spectra taken at 300, 140, and 75 K (indicated by the thick solid curves) for $x = 0.2$. Each of the V $2p$ spectra is corrected with Shirley-type background excluding O1s with reference to Silversmith *et al.* [31], and is fitted to five Voigts (mixture of Gaussian and Lorentzian). The V $2p_{3/2}$ peak can be decomposed with V^{2+} and V^{3+} contributions, which are included in the fit considering the fact that the average V valence of $Ba_{1-x}Sr_xV_{13}O_{18}$ is $\sim +2.62$. From V $2p_{3/2}$, the V^{2+} peak is fitted with two Voigts and V^{3+} is fitted with one Voigt. In V $2p_{1/2}$, each V^{2+} and V^{3+} component is fitted with one Voigt, respectively. The energy separation between the V^{3+} and V^{2+} components in all temperatures is large compared to the typical values [32,33]. In the V $2p$ HAXPES of various metallic V oxides such as $SrVO_3$ [34], VO_2 (metallic phase) [35], and V_2O_3 (metallic phase) [32,33,36–38], it has commonly been reported that the V $2p_{3/2}$ peaks are very broad and are extended from 519 to 512 eV. At

75 K, the low binding energy side of the V $2p_{3/2}$ branch reaches 512 eV. Also, broadening due to phonons [38] is possible. We also tried curve fittings with five Voigts similarly as described earlier and four Doniach-Sunjic profiles on the V $2p$ spectra with the Shirley background removed from the broad region including O $1s$ [31]. The estimated V^{2+}/V^{3+} intensity ratio is summarized in Table I. As for the Doniach-Sunjic fitting, the asymmetric parameter is set to the same as that obtained from O $1s$ for each temperature (see Supplemental Material [30]). At 300 K, the V $2p_{3/2}$ peak becomes less broad and is relatively shifted towards higher binding energy. The V $2p$ binding energy decreases with cooling and may be related with band bending in the interface of the coexisting phases [39]. The intensity ratio between the low-energy and high-energy components, which correspond to the V^{2+} and V^{3+} components, is obtained from fitted results of V $2p_{3/2}$ rather than V $2p_{1/2}$ since the V $2p_{1/2}$ peak overlaps with the

TABLE I. Intensity ratio V^{2+}/V^{3+} in $Ba_{1-x}Sr_xV_{13}O_{18}$ for $(x = 0, 0.2, 1)$ at different phases across the transitions. V1: Voigt profile on V $2p$ corrected with Shirley background excluding O $1s$ region; V2: Voigt profile on V $2p$ corrected with Shirley background including O $1s$ region; DS: Doniach-Sunjic profile on V $2p$ corrected with Shirley background including O $1s$ region [31].

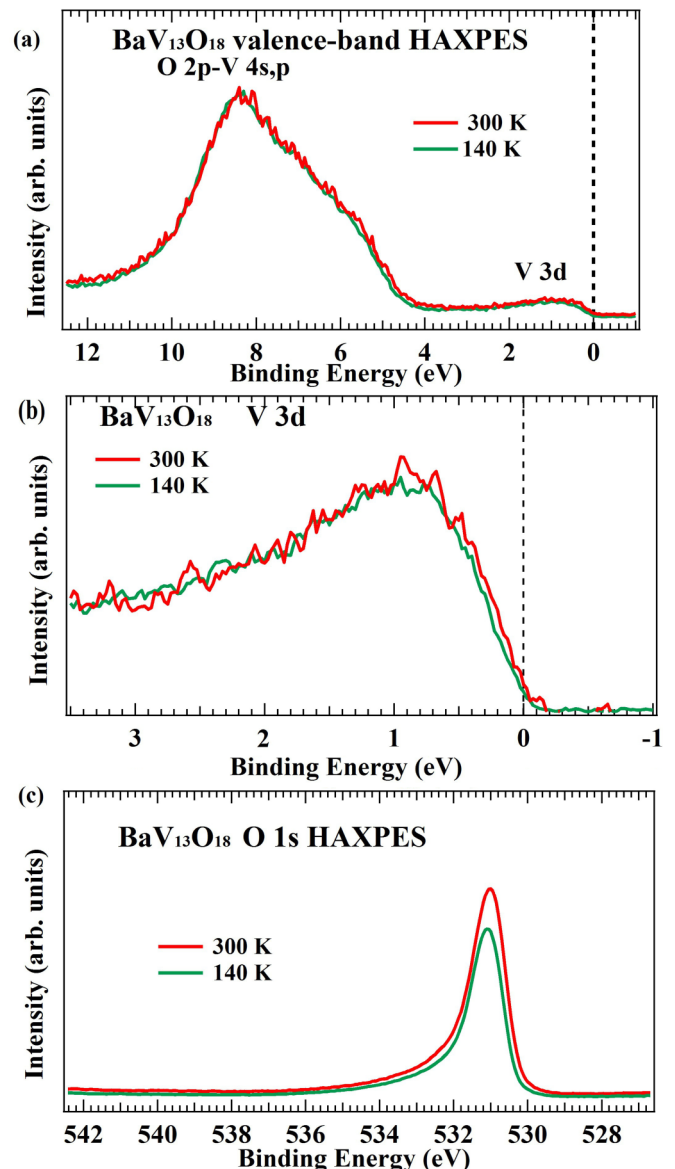| Fittings	T (K)	V^{2+}/V^{3+} ratio in $Ba_{1-x}Sr_xV_{13}O_{18}$		
		$x = 0$	$x = 0.2$	$x = 1$
V1	300	0.62	0.64	0.64
	140	0.64	0.64	
	75		0.62	0.79
V2	300	0.64	0.64	0.68
	140	0.64	0.65	
	75		0.67	0.81
DS	300	0.72	0.71	0.60
	140	0.70	0.74	
	75		0.68	0.82

FIG. 5. HAXPES spectra of $BaV_{13}O_{18}$ at 300 and 140 K for (a) valence band, (b) V $3d$, and (c) O $1s$.

charge-transfer satellites of the V $2p_{3/2}$ peak in V oxides [40]. The intensity ratio between V^{2+} and V^{3+} fluctuates around 0.6 at the temperatures across the phase transitions and is shown in Table I. The values are found consistent for the charge order or fluctuation with average valency of +2.62 or V^{2+} : V^{3+} = 5 : 8. This leads to the suppression of the spectral weight at the Fermi level.

The temperature dependence of magnetic susceptibility χ is schematically drawn in Fig. 2(d). The reduction in magnetic susceptibility χ in the trimer phase can be understood on the basis of the charge fluctuation of V^{2+} and V^{3+} associated with the competition between tetramerization and trimerization. Since the V^{2+} and V^{3+} components are well separated in the V $2p$ HAXPES taken at 300 K (Fig. 4), two (or one) V^{2+} and two (or three) V^{3+} form the tetramer at 300 K and a kind of Zener double-exchange interaction provides ferromagnetic coupling between the V^{2+} and V^{3+} sites and χ can be enhanced [7]. The magnetic susceptibility χ decreases slowly with cooling until T_{co} and increases up to T_{tr} like Curie-Weiss behavior that is assigned to the localized V $3d$ electron at the central site [6]. Here, it should be noted that one cannot exclude the possibility of one V^{4+} among 13 V sites in the present analysis since the V^{3+} peak is extremely broad. Below T_{tr}, χ falls down sharply, as seen in Fig. 2(d), because the charge-order phase breaks down and χ is somehow reduced with trimerization

where spin-singlet states between V^{3+} and V^{3+} are realized in some of the trimers. However, most of the trimers are constructed from V^{2+} and V^{3+} with ferromagnetic coupling and contribute to the residual component of χ. Below 75 K, the increase in χ is already ascribed to impurity spin of the sample [6].

Figures 5(a) and 5(b) show the valence-band HAXPES spectra of BaV$_{13}$O$_{18}$ across the charge-order transition. At 140 K, spectral weight at the Fermi level is relatively dropped compared to 300 K. This agrees with the increases of resistivity at 140 K, as shown in Fig. 2(b). The presence of localized electrons at the central V site surrounded with tetramers could be the common origin of such behavior in the charge-order phase. Also, the Seebeck coefficient is negative at room temperature and its absolute value further increases with lowering temperature, as seen from Fig. 2(c). This can be associated to the relative increase of the V $3d$ and O $1s$
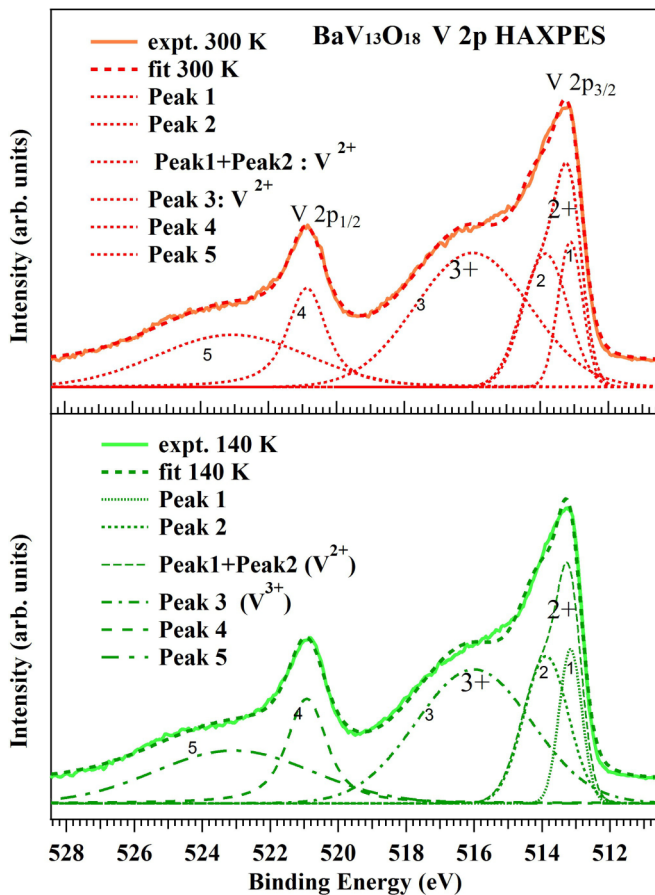

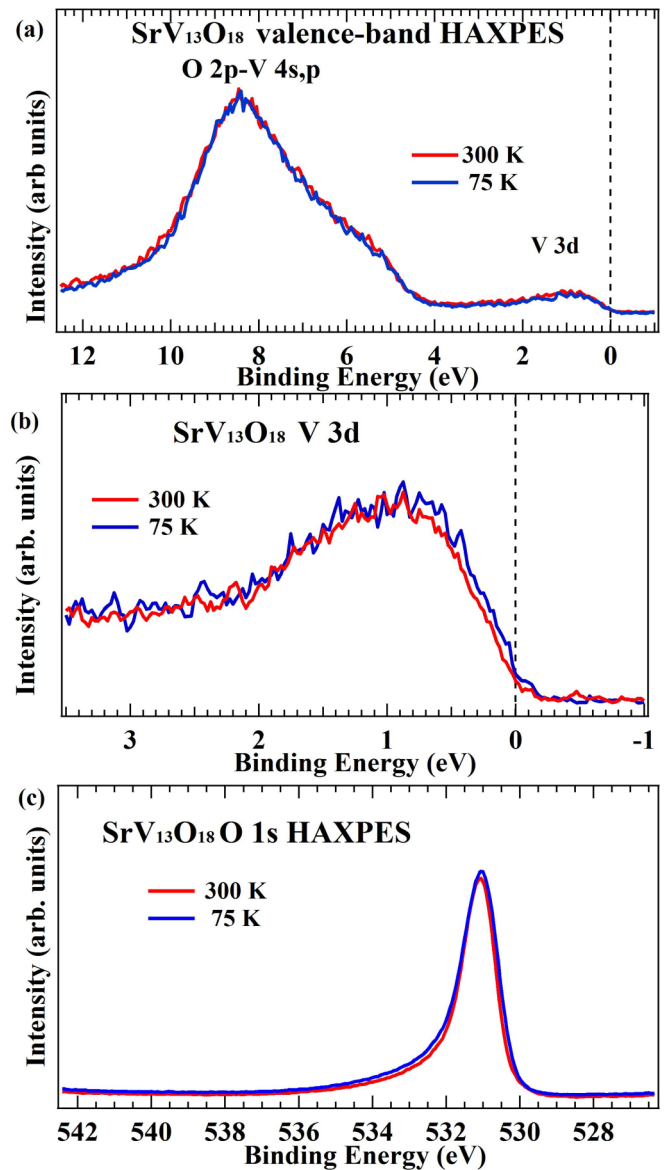FIG. 6. V $2p$ HAXPES spectra fitted with five Voigt functions for 300 and 140 K. Peaks 1 and 2 represent V^{2+}, and peak 3 represents the V^{3+} component in V $2p_{3/2}$. Peaks 4 and 5 are fitted for the V $2p_{1/2}$ region.

FIG. 7. HAXPES spectra of SrV$_{13}$O$_{18}$ at 300 and 75 K for (a) valence band, (b) V $3d$, and (c) O $1s$.
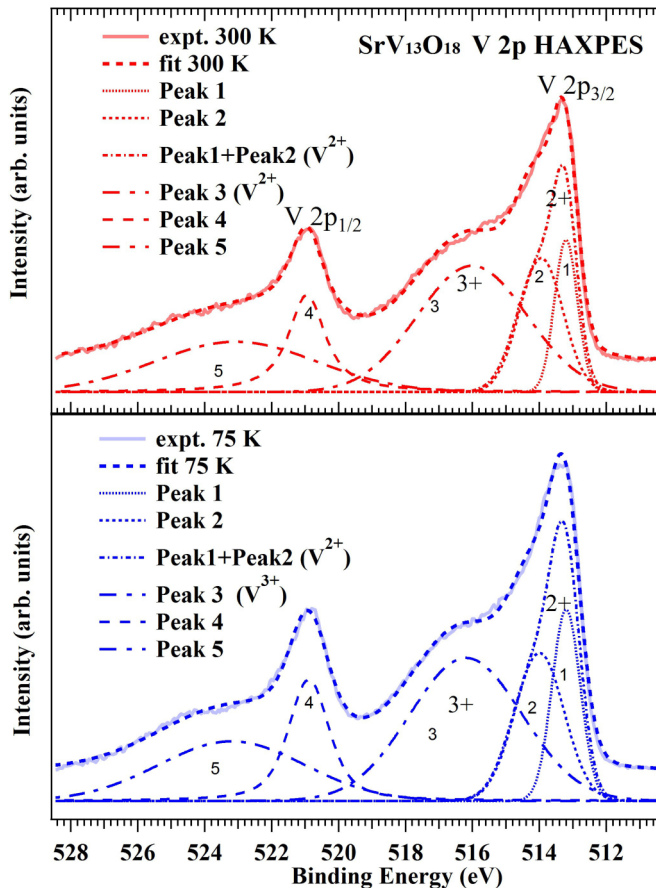
FIG. 8. V $2p$ HAXPES spectra fitted with five Voigt functions for 300 and 75 K. Peaks 1 and 2 represent V^{2+}, and peak 3 represents the V^{3+} component in V $2p_{3/2}$. Peaks 4 and 5 are fitted for the V $2p_{1/2}$ region.

binding energies with cooling seen in Figs. 5(b) and 5(c). Figure 6 shows the V $2p$ HAXPES spectra taken at 300 and 140 K (indicated by the thick solid curves). Each of the V $2p$ spectra at both temperatures is corrected with Shirley-type background and fitted to five Voigts similarly as described above for $Ba_{0.8}Sr_{0.2}V_{13}O_{18}$. From the fit parameters, the low binding energy peak of the V $2p_{3/2}$ at 300 K is relatively broader and shifted towards lower binding energy compared to the spectrum at 140 K. The intensity ratio between the low-energy and high-energy components, which correspond to the V^{2+} and V^{3+} components fluctuates around 0.6–0.7 at different temperatures, is obtained from the Voigt fits and the Doniach-Sunjic fits (see Supplemental Material [30]), as shown in Table I. The behavior of magnetic susceptibility around 140 K, as seen in the schematic of the phase diagram in Fig. 2(d), could be related to the central V atom of the hexagonal plane and the charge order with $V^{2+} : V^{3+} = 5 : 8$.

Figures 7(a) and 7(b) show the valence-band HAXPES spectra of $SrV_{13}O_{18}$ collected above and much below T_{tr}. The resistivity drops below $T_{tr} \approx 250$ K, where the $3d$ electrons become itinerant as explained earlier [6]. A relative increase in spectral weight at the Fermi level of $SrV_{13}O_{18}$ is seen at 75 K [Fig. 7(b)] as a signature of the metallic nature due to the presence of $3d$ itinerant electrons. However, the higher charge

fluctuation at 75 K (Table I) suppresses the spectral weight at the Fermi level in comparison to the case of $Ba_{0.8}Sr_{0.2}V_{13}O_{18}$. In Fig. 7(c), the O $1s$ HAXPES of the metallic phase at 75 K exhibits the slight increase of asymmetry due to the screening effect from such itinerant $3d$ electrons. The relative increase in spectral weight at the Fermi level can be compared with the decrease in resistivity [Fig. 2(b)] and the behavior of the Seebeck coefficient [Fig. 2(c)]. Figure 8 shows the V $2p$ HAXPES spectra taken at 300 and 75 K (indicated by the thick solid curves). The V $2p$ spectrum at each temperature is fitted to five Voigts similarly as described earlier. The intensity ratio between the low-energy and high-energy components which correspond to the V^{2+} and V^{3+} components obtained from the Voigt fits increases from 0.64 for 300 K to 0.79 for 75 K, as shown in the section V1 in Table I. The increase is also seen with the other set of fittings, as shown in the sections V2 and DS in Table I. This shows that charge fluctuation in the trimer phase is different between $x = 0.2$ and $x = 1$. At $x = 0.2$, the V^{2+} peak becomes broad at 75 K without drastic change of the intensity ratio. Therefore, the itinerant electrons are derived from extra electrons at the V^{2+} site and/or extra holes at the V^{3+} site, and the population of the V^{2+} and V^{3+} sites is almost locked. On the other hand, at $x = 1$, the intensity ratio between the V^{2+} and V^{3+} peaks is changed at 75 K without broadening of the peak. Therefore, although the population of the V^{2+} and V^{3+} sites is flexible at $x = 1$, the carriers are rather localized and a kind of polaronic transport would be responsible for the metallic behavior. This is consistent with the valance-band HAXPES in which the spectral weight suppression in the trimer phase is different between $x = 0.2$ and 1.

IV. CONCLUSIONS

We conclude that core-level HAXPES measurements have shown the unusual metallic states with mixed valence between V^{2+} and V^{3+} in the series of $x = 0, 0.2, 1$ in $Ba_{1-x}Sr_xV_{13}O_{18}$. The $V^{2+/3+}$ charge fluctuation or charge order is confirmed in the V $2p$ core-level HAXPES results. This charge fluctuation or charge order suppresses the spectral weight at the Fermi level and creates the pseudogap as observed in the valence-band HAXPES. The valence-band HAXPES results are almost consistent with the transport behaviors seen across the transitions. Although the pseudogap remains probably due to the charge fluctuation, the spectral weight at the Fermi level is slightly enhanced for the presence of $3d$ itinerant electrons at the low-temperature trimer phase. In general, various physical properties across the transition of $AV_{13}O_{18}$ ($A = $ Ba, Sr), and $Ba_{0.8}Sr_{0.2}V_{13}O_{18}$ are well ascribed to the charge fluctuation of V^{2+} and V^{3+}, which would be related to the competition between the tetramer and trimer phases.

[1] M. Imada, A. Fujimori, and Y. Tokura, Rev. Mod. Phys. **70**, 1039 (1998).

[2] D. I. Khomskii, *Transition Metal Compounds* (Cambridge University Press, Cambridge, 2014).

[3] G. Liu and J. E. Greedan, J. Solid State Chem. **122**, 416 (1996).

[4] C. A. Bridges and J. E. Greedan, J. Solid State Chem. **177**, 1098 (2004).

[5] M. Ikeda, Y. Nagamine, S. Mori, J. E. Kim, K. Kato, M. Takata, and T. Katsufuji, Phys. Rev. B **82**, 104415 (2010).

[6] M. Ikeda, T. Okuda, K. Kato, M. Takata, and T. Katsufuji, Phys. Rev. B **83**, 134417 (2011).

[7] T. Yoshino, M. Okawa, T. Kajita, S. Dash, R. Shimoyama, K. Takahashi, Y. Takahashi, R. Takayanagi, T. Saitoh, D. Ootsuki, T. Yoshida, E. Ikenaga, N. L. Saini, T. Katsufuji, and T. Mizokawa, Phys. Rev. B **95**, 075151 (2017).

[8] T. Kajita, T. Kanzaki, T. Suzuki, J. E. Kim, K. Kato, M. Takata, and T. Katsufuji, Phys. Rev. B **81**, 060405(R) (2010).

[9] A. V. Mahajan, D. C. Johnston, D. R. Torgeson, and F. Borsa, Phys. Rev. B **46**, 10973 (1992).

[10] G. Jackeli and G. Khaliullin, Phys. Rev. Lett. **101**, 216804 (2008).

[11] Y. Ishige, T. Sudayama, Y. Wakisaka, T. Mizokawa, H. Wadati, G. A. Sawatzky, T. Z. Regier, M. Isobe, and Y. Ueda, Phys. Rev. B **83**, 125112 (2011).

[12] A. C. Gossard, J. P. Remeika, T. M. Rice, H. Yasuoka, K. Kosuge, and S. Kachi, Phys. Rev. B **9**, 1230 (1974).

[13] A. S. Botana, V. Pardo, D. Baldomir, A. V. Ushakov, and D. I. Khomskii, Phys. Rev. B **84**, 115138 (2011).

[14] K. Takubo, T. Kanzaki, Y. Yamasaki, H. Nakao, Y. Murakami, T. Oguchi, and T. Katsufuji, Phys. Rev. B **86**, 085141 (2012).

[15] Y. Shimizu, K. Matsudaira, M. Itoh, T. Kajita, and T. Katsufuji, Phys. Rev. B **84**, 064421 (2011).

[16] H. F. Pen, J. van den Brink, D. I. Khomskii, and G. A. Sawatzky, Phys. Rev. Lett. **78**, 1323 (1997).

[17] A. Nogami, K. Takubo, T. Kajita, M. Hoshino, and T. Katsufuji, Phys. Rev. B **84**, 214442 (2011).

[18] T. Kanzaki, R. Kubota, and T. Katsufuji, Phys. Rev. B **85**, 144410 (2012).

[19] K. Iwasaki, H. Takizawa, K. Uheda, T. Endo, and M. Shimada, J. Solid State Chem. **158**, 61 (2001).

[20] K. Iwasaki, H. Takizawa, H. Yamane, S. Kubota, J. Takahashi, K. Uheda, and T. Endo, Mater. Res. Bull. **38**, 141 (2003).

[21] K. Momma and F. Izumi, J. Appl. Crystallogr. **44**, 1272 (2011).

[22] T. Katsufuji, T. Okuda, R. Murata, T. Kanzaki, K. Takayama, and T. Kajita, J. Phys. Soc. Jpn. **85**, 013703 (2016).

[23] E. Ikenaga, M. Kobata, H. Matsuda, T. Sugiyama, H. Daimon, and K. Kobayashi, J. Electron Spectrosc. Relat. Phenom. **190**, 180 (2013).

[24] S. Ouardi, G. H. Fecher, and C. Felser, J. Electron Spectrosc. Relat. Phenom. **190**, 249 (2013).

[25] K. Kobayashi, M. Yabashi, Y. Takata, T. Tokushima, S. Shin, K. Tamasaku, D. Miwa, T. Ishikawa, H. Nohira, T. Hattori, Y. Sugita, O. Nakatsuka, A. Sakai, and S. Zaima, Appl. Phys. Lett. **83**, 1005 (2003).

[26] K. Kobayashi, Nucl. Instr. Meth. Phys. Res. A **601**, 32 (2009).

[27] K. Kobayashi, Nucl. Instr. Meth. Phys. Res. A **547**, 98 (2005).

[28] M. Sacchi, F. Offi, P. Torelli, A. Fondacaro, C. Spezzani, M. Cautero, G. Cautero, S. Huotari, M. Grioni, R. Delaunay, M. Fabrizioli, G. Vankó, G. Monaco, G. Paolicelli, G. Stefani, and G. Panaccione, Phys. Rev. B **71**, 155117 (2005).

[29] J. J. Yeh and I. Lindau, Atom. Data Nucl. Data Tables **32**, 1 (1985).

[30] See Supplemental Material at http://link.aps.org/supplemental/10.1103/PhysRevB.95.195116 doi for fittings with Doniach-Sunjic profiles.

[31] G. Silversmit, D. Depla, H. Poelman, G. B. Marin, and R. D. Gryse, J. Electron Spectrosc. Relat. Phenom. **135**, 167 (2004).

[32] G. A. Sawatzky and D. Post, Phys. Rev. B **20**, 1546 (1979).

[33] M. C. Biesinger, L. W. M. Lau, A. R. Gerson, and R. St. C. Smart, Appl. Surf. Sci. **257**, 887 (2010).

[34] J. Laverock, J. Kuyyalil, B. Chen, R. P. Singh, B. Karlin, J. C. Woicik, G. Balakrishnan, and K. E. Smith, Phys. Rev. B **91**, 165123 (2015).

[35] S. Suga, A. Sekiyama, S. Imada, T. Miyamachi, H. Fujiwara, A. Yamasaki, K. Yoshimura, K. Okada, M. Yabashi, K. Tamasaku, A. Higashiya, and T. Ishikawa, New J. Phys. **11**, 103015 (2009).

[36] G. Panaccione, M. Sacchi, P. Torelli, F. Offi, G. Cautero, R. Sergo, A. Fondacaro, C. Henriquet, S. Huotari, G. Monaco, and L. Paolasini, J. Electron Spectrosc. Relat. Phenom. **156-158**, 64 (2007).

[37] T. Uozumi, K. Okada, A. Kotani, R. Zimmermann, P. Steiner, S. Hener, Y. Tezuka, and S. Shin, J. Electron Spectrosc. Relat. Phenom. **83**, 9 (1997).

[38] P. H. Citrin, P. Eisenberger, and D. R. Hamann, Phys. Rev. Lett. **33**, 965 (1974).

[39] Z. Zhang and J. T. Yates, Jr., Chem. Rev. **112**, 5520 (2012).

[40] A. E. Bocquet, T. Mizokawa, K. Morikawa, A. Fujimori, S. R. Barman, K. Maiti, D. D. Sarma, and Y. Tokura, and M. Onoda, Phys. Rev. B **53**, 1161 (1996).